DOI 10.1007/s12182-009-0021-0

Anisotropic characteristics of electrical responses of fractured reservoir with multiple sets of fractures

Shen Jinsong[1, 2, 3]*, Su Benyu[1] and Guo Naichuan[1]

[1] Department of Geophysics, School of Resource and Information Technology, China University of Petroleum, Beijing 102249, China

[2] Key Laboratory of CNPC Geophysical Exploration, China University of Petroleum, Beijing 102249, China

[3] State Key Laboratory of Petroleum Resource and Prospecting, China University of Petroleum, Beijing 102249, China

Abstract: In fractured reservoirs, the fractures not only provide the storage space for hydrocarbons, but also form the main flow channels which connect the pores of the matrix, so fractures dominate the productivity of reservoirs. However, because of the heterogeneity and randomness of the distribution of fractures, exploration and evaluation of fractured reservoirs is still one of the most difficult problems in the oil industry. In recent years, seismic anisotropy has been applied to the assessment of fractured formations, whereas electrical anisotropy which is more intense in fractured formations than seismic anisotropy has not been studied or used so extensively. In this study, fractured reservoir models which considered multiple sets of fractures with smooth and partly closed, rough surfaces were established based on the fractures and pore network, and the vertical and horizontal electrical resistivities were derived as a function of the matrix and fracture porosities according to Ohm's law. By using the anisotropic resistivity equations, variations of the electrical anisotropy of three types of fractured models under the conditions of free pressure and confining pressure were analyzed through the variations of the exerted pressure, matrix porosity, fracture aperture and formation water resistivity. The differences of the vertical and horizontal resistivities and the anisotropy between the connected and non-connected fractures were also analyzed. It is known from the simulated results that an increase of the confining pressure causes a decrease of electrical anisotropy because of the elasticity of the closed fractures and the decrease of the fracture aperture. For a fixed fracture porosity, the higher the matrix porosity, the weaker the electrical anisotropy in the rock formation.

Key words: Fractured reservoir, partly closed fracture, electrical anisotropy, fracture roughness

1 Introduction

Fractured reservoirs are one of the most important types of hydrocarbon-bearing reservoirs. More than 60% of the world's oil reserves and 40% of the gas reserves are held in fractured carbonate reservoirs (Lucia, 2007). Most fractured reservoirs are naturally fractured and contain fractures that range from isolated microscopic fissures to kilometer-long structures called fracture swarms or corridors. The fractures create complex paths for hydrocarbons and other fluids which affect the reservoir characteristics, production performance, and ultimate oil and gas recovery (Lucia, 2007; Minh et al, 2007). In recent years, it has been extensively recognized in the oil industry that the application of geophysical exploration to the prediction and evaluation of the subsurface fractured formation is effective and economic (Colin, 2007; Meju et al, 2001; Meju, 2002). Fractured reservoirs are widely distributed all over the world. There are lots of fractured carbonate reservoirs of a large scale in the Middle East and other regions (Lucia, 2007). In China, fractured reservoirs have been found in Sichuan, Xinjiang, Qinghai, Dagang, Daqing and most oilfields in southern China.

However, because of the low porosity and complex pore structure in fractured formations, the prediction and evaluation of the distribution of fractures has been a difficult but important problem in the oil industry. In hydrology and civil engineering geology, identification and quantitative evaluation of fracture distribution also has important significance to the simulation of fluid flow and pollution diffusion in the subsurface formation.

In hydrology and engineering geology, the characteristics of the fluid flow in the subsurface formations are mainly studied by drilling and fluid flow experiments in boreholes, such as inter-well interference and tracing. All these methods are of high cost and have to destroy the structure balance of the fracture system. In the oil industry, fracture evaluation at present is mainly based on core analysis, geophysical well logging, seismic exploration (Horne, 2003; Tryggvason and Linde, 2006; Shaw and Sen, 2004; 2006), and electromagnetic exploration (Ritzi and Andolsek, 1992; Carpenter et al, 1994; Al Hagrey, 1994; Cohn and Rudman, 1995). Thomsen (1986)

*Corresponding author. email: shenjinsong@cup.edu.cn
Received October 28, 2008

and Chapman (2003) studied elastic anisotropy in porous media with a parallel fracture distribution and the sensitivity of seismic responses to the geometric parameters of fractures. Their achievements sparked a boom in investigation of fracture prediction using seismic data.

Electrical well logging is widely used in the assessment of fractured reservoirs in the oil industry (Standen et al, 1993; Tetsuya et al, 2002; Luthi and Souhaite, 1990). For example, micro-resistivity scanning has been used as an important tool in the description of borehole wall fractures. Surface electrical surveys have also been widely applied to evaluating the fracture distribution in hydrology and engineering geology (Busby, 2000; Lane et al, 1995; Meju et al, 2001; Boadu et al, 2005). In spite of the validity of surface electrical surveys, there are still lots of problems about the conductivity mechanism and characteristics of theoretical responses that have not been understood completely in fracture evaluation. Therefore, it is essential that the electrical responses and corresponding theoretical relations should be set up based on a typical fracture model for accurate interpretation of the electrical survey data.

In this study, fractured reservoir models, which considered multiple sets of horizontal and vertical fractures with smooth surfaces and partly closed, rough surfaces respectively were established based on fractures and pore network. The equations of vertical and horizontal electrical resistivities were derived on the basis of the fractured reservoir models. By using the response equations, the variations of the horizontal and vertical resistivities and the electrical anisotropy of the fractured models under the conditions of free pressure and confining pressure were analyzed as a function of the fracture aperture, fracture density and closed roughness. The characteristics of the electrical resistivity and the anisotropy of a closed, rough fracture model were analyzed as a function of matrix porosity. The results are helpful for quantitative fracture evaluation and prediction. To simplify the discussion, we ignored the conductivity and corresponding polarization effect of fracture and pore surfaces on electrical anisotropy. For the conductivity of the porous rock matrix, the first order approximation of the Hanai-Bruggeman conductivity model (Bussian, 1983; Berg, 1995) was applied to calculating the resistivity of the porous matrix.

2 Hanai-Bruggeman conductivity model of porous rock matrix

Fractured formations usually have a low porosity of rock matrix, and the fractures provide the storage space for fluids, and form the main flow channels that connect the pores of the matrix. The classic Archie equation (Archie, 1942) deduced from clean sand core data becomes ineffective in fractured reservoirs with a low matrix porosity (Bussian, 1983). Here, we used the Hanai-Bruggeman conductivity model modified by Bussian (1983) and Berg (1995) as a basic equation, and derived its first order approximation under appropriate constraints, which can be suitable for estimation of the resistivity of the porous matrix in fractured formations. The conductivity of the formation saturated with saline water (Bussian, 1983; Berg, 1995) can be expressed as:

$$\begin{aligned}\sigma_0 &= \sigma_w \phi^m \left(\frac{1-\sigma_s/\sigma_w}{1-\sigma_s/\sigma_0}\right)^m \\ &= \sigma_w \phi^{m/(1-m)} \left(\frac{1-\sigma_w/\sigma_s}{1-\sigma_0/\sigma_s}\right)^{m/(1-m)}\end{aligned} \tag{1}$$

where σ_s is the conductivity of the grain in matrix, σ_w is the conductivity of the formation water, ϕ is the matrix porosity, and m is the geometric factor related to the tortuosity of the matrix pores.

From Eq. (1), it is evident that the resistivity of the formation saturated with saline water can be rewritten as:

$$\frac{1}{\rho_{rb}} = \frac{1}{\rho_f} \phi^{m/(1-m)} \left(\frac{1-\rho_s/\rho_f}{1-\rho_s/\rho_{rb}}\right)^{m/(1-m)} \tag{2}$$

where ρ_{rb} is the resistivity of the porous matrix, ρ_s is the resistivity of the grain in matrix rock, and ρ_f is the resistivity of formation water.

It should be noted that Eq. (2) is superior to Archie equation since the resistivity of the matrix grain ρ_s has a limited value and Eq. (2) can also be applied to shaly sand formations and formations with conductive minerals in the matrix. To check the validity of Eq. (2), a shaly sand model with pores and spherical grain matrix was used as a sample. In this sample, m was set to be 2, hence two positive and negative roots were obtained. Fig. 1 shows the results of the first order approximation (H-Bnon), and the two reference solutions from Waxman-Smits (1968) (noted as W-Sext) and Archie equations (Archie, 1942) (noted as Archie). From the results in Fig. 1, it is known that in this shaly sand model, the Archie law can only be held correct for high salinity of formation water which corresponds to high conductivity of water, whereas the Waxman-Smith equation is more suitable for low salinity of formation water which shows evident additional conductivity resulting from the shale content. The first order approximation (H-Bnon) is consistent with the Archie law at the high salinity of water and fits well with Waxman-Smith equation at the low salinity of water. Moreover, it fills the gap between the high salinity and low salinity of water which generally results in inaccurate formation evaluation.

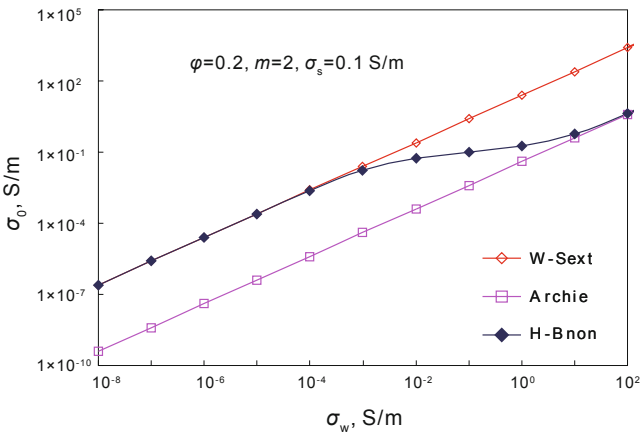

Fig. 1 Comparison among the results from the Hanai-Bruggeman conductivity model, Archie equation and Waxman-Smith equation

3 Electrical responses of the horizontal fracture model

Here, we discuss the model with multiple sets of horizontal fractures and porous matrix, and both the pores and fractures are filled with the same saline formation water. For simplification, the effects of the conductivity and polarization of the fracture and pore surfaces on the electrical anisotropy are ignored (Brace and Orange, 1968). For the fractures filled with conductive minerals, the resistivity is simplified to the equivalent formation water resistivity, and for the fractures filled with non-conductive minerals, the resistivity is taken as that of the equivalent closed rings developed in the fractures.

3.1 Model of multiple sets of fractures with horizontal surfaces

We consider a fractured formation with multiple sets of fractures with horizontal surfaces shown in Fig. 2(a) and with partly closed, rough surfaces shown in Fig. 2(b). The section area of the fracture model is A, the fracture aperture of the i^{th} fracture $e_i = e$, the extending width of each fracture is $w_i = w$, the length of the rock is L, and the closed portion of the rough surfaces is α. Therefore, the horizontal and vertical resistivities of the fractured formation with fractures of total number n are as follows (Appendix A):

$$R_h = \frac{\rho_{rb}\rho_f}{(\rho_{rb}-\rho_f)new/A+\rho_f}$$
$$R_v = \rho_{rb} + \frac{new(\rho_f-\rho_{rb})}{A} \quad (3)$$

where n is the total number of fractures, e is the fracture aperture and w is the extending width of fracture, and ρ_f is the fracture fluid resistivity. We only consider fractures filled with formation water, that is, $\rho_f = R_w = 1/\sigma_w$ (reciprocal of the water conductivity), in inverse of S/m, ρ_{rb} is the resistivity of the formation saturated with water, in inverse of S/m. In the following derivations, R_w is taken as fluid resistivity instead of ρ_f.

Fig. 3 indicates that the anisotropic coefficient is related to fracture aperture and matrix porosity. Comparing Fig. 3(a) with Fig. 3(b), it is understood that, under specific conditions, high-density fractured formation with low matrix porosity φ, that is corresponding to high fracture porosity, shows significant electrical anisotropy. With the increase of matrix porosity and the decrease of fracture porosity, the electrical anisotropic coefficient decreases rapidly. Therefore, in case of very low fracture porosity, the effect of fractures on electrical anisotropy can be ignored in the interpretation of electrical survey data.

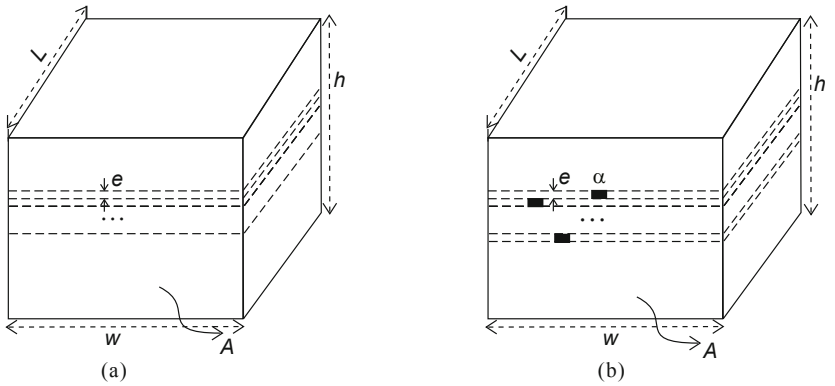

Fig. 2 Formation model of multiple horizontal fractures. (a) fractures with horizontal surfaces, (b) fractures with partly closed, rough surfaces

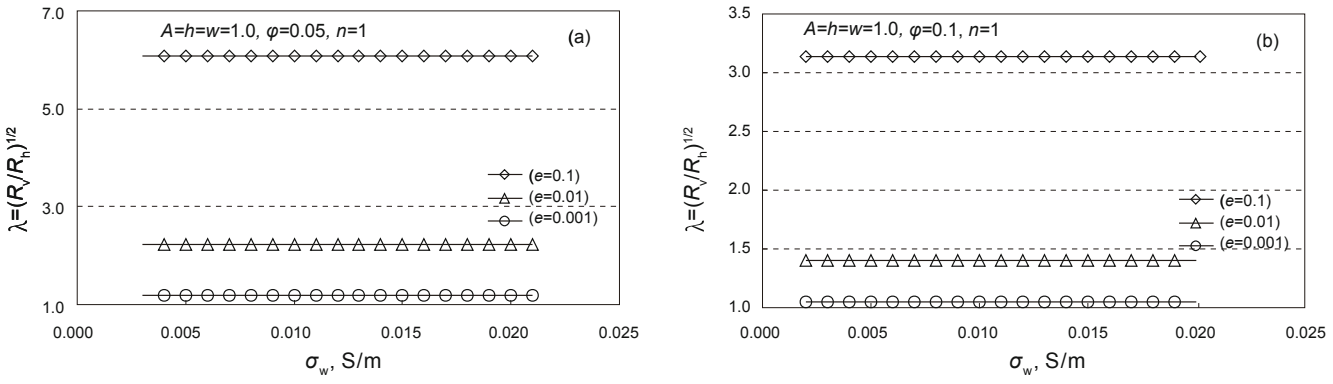

Fig. 3 Variation of the electrical anisotropy of a formation with a single horizontal fracture of variable aperture with various matrix porosities. (a) matrix porosity φ=0.05, (b) matrix porosity φ=0.1

3.2 Model of multiple sets of fractures with closed, rough surfaces

Considering the fractured model of multiple sets of fractures with closed, rough surfaces in Fig. 2(b), when the roughness, which describes the height of the irregularity of the fracture surfaces, is extremely small compared to the fracture aperture e_i, the conductivity contribution of the fractures can be approximated by fractures with horizontal surfaces and average fracture aperture (Stesky, 1986). If the roughness is very large and approaches the fracture aperture, fractures show the features of partly closed surfaces and low conductivity. Walsh (1981) took advantage of the similarity of the fluid flow path and the electrical current path in closed, rough fractures, and developed an effective electrical model which comprised of insulating rings in horizontal fractures, as shown in Fig. 2(b). In the model, it is assumed that formation water in fractures is separated by the insulating rings (Walsh, 1981), and the effective resistivity of the fracture can be approximated by the following equation:

$$\langle \rho_f \rangle = R_w(1+\alpha)/(1-\alpha) \tag{4}$$

where $\langle \rho_f \rangle$ is the effective resistivity of a specific fracture filled with formation water clogged by insulating rings, α is the portion of the closed area accounting for the total area of the fracture surfaces. Substituting ρ_f with $\langle \rho_f \rangle$ in Eq. (3), we can obtain equations of horizontal and vertical resistivities of closed, rough fractured formation:

$$\begin{aligned} R_h &= \frac{\rho_r R_w(1+\alpha)/(1-\alpha)}{\left[\rho_r - R_w(1+\alpha)/(1-\alpha)\right] new/A + R_w(1+\alpha)/(1-\alpha)} \\ R_v &= \rho_r + \frac{new\left[R_w(1+\alpha)/(1-\alpha) - \rho_r\right]}{A} \end{aligned} \tag{5}$$

Fig. 4 shows the electrical anisotropy coefficients changing with matrix porosity, fracture porosity (also shown by the total fracture number n in a specific sample length) and the closed roughness. From Fig. 4(a), it is known that whether the fracture surfaces are rough or not, the electrical anisotropy becomes weaker with the increase of the matrix porosity corresponding to a small proportion of fracture porosity. For a specific matrix porosity, with the increase of fracture porosity φ_f, fractured formation with closed contact shows non-linear increase of electrical anisotropy, whereas the formation with smooth fracture surfaces shows linear increase of electrical anisotropy. In Fig. 4(b), it is shown that electrical anisotropy shows a sharp decrease when the formations include closed fracture surfaces with the increase of the matrix porosity. Moreover, both cases show that electrical anisotropy can be above 15 when the fracture porosity dominates formation porosity.

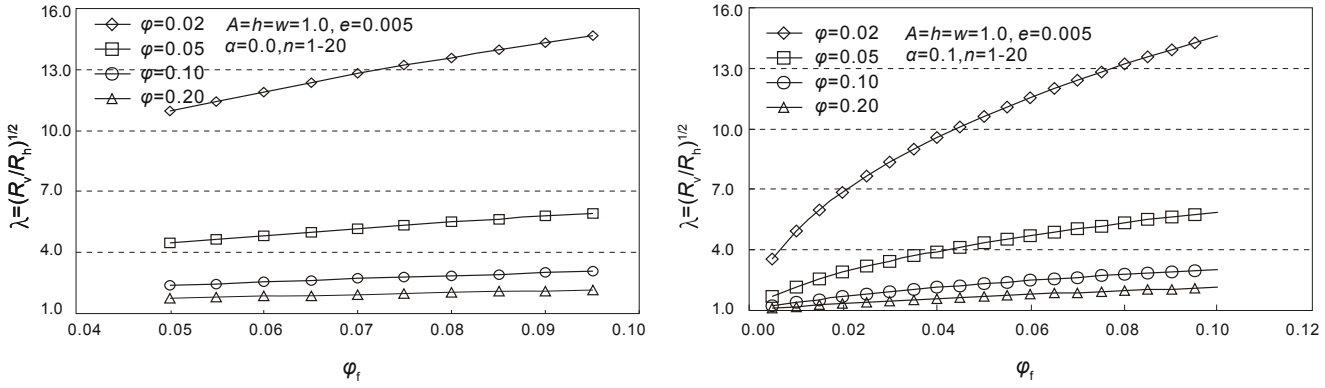

Fig. 4 Variation of the electrical anisotropy with matrix porosity, fracture porosity and closed contact area in a formation with horizontal fractures of fixed aperture. (a) horizontal fracture surfaces with α=0.0, (b) rough fracture surfaces with α=0.1

4 Electrical anisotropy of fractured formation with rough fracture surfaces under confining pressure

Under confining pressure, the fracture aperture and closed roughness vary with confining pressure, and thus affect the formation resistivity. Provided that the variations of section area A and width w are very small and can be ignored, and the fluid flow in the fractures accords with the Darcy law, Walsh (1981) developed approximate relations for fracture aperture and closed roughness with confining pressure. If the elastic deformation varies linearly with the confining pressure, and the closed contact medium is elastic, we can obtain:

$$\mathrm{d}e/\mathrm{d}p = \sqrt{2}\theta/p\,, \quad \mathrm{d}\alpha/\mathrm{d}p = b \tag{6}$$

where θ is the standard deviation of the fracture closed roughness, b is the elastic coefficient of the fractured formation, p is the stress normal to the fracture surfaces in case of the anisotropic formation.

In fact, Eq. (6) is an empirical relation of the fracture aperture and closed roughness assuming that the closed roughness has an exponent function distribution (Brown, 1995; Linde et al, 2006), and it is an linear approximation of the variation of e and α as follows:

$$e = e_0 - \sqrt{2}\theta \ln(p/p_0)\,, \quad \alpha = \alpha_0 + b(p - p_0) \tag{7}$$

where e_0 and α_0 are the initial fracture aperture and closed roughness when the confining pressure is p_0.

Substituting e and α in Eq. (5) with those in Eq. (7), the equations of horizontal and vertical resistivities of closed, rough fractured formation under confining pressure can be obtained.

Fig. 5 shows resistivities and electrical anisotropy of a fractured formation with a single set and multiple sets of closed rough fractures changing with confining pressure. In Fig. 5(a) and Fig. 5(b), it is known that the horizontal and vertical resistivities increase non-linearly with the increase of confining pressure which causes a higher proportion of closed contact areas in the fractures, and the electrical anisotropy shows a non-linear decreasing trend. Moreover, the horizontal resistivity increases faster than that of the vertical resistivity. It can be concluded that for a specific fracture porosity, the denser the fractures and the smaller the fracture aperture, the weaker the electrical anisotropy with the increase of confining pressure.

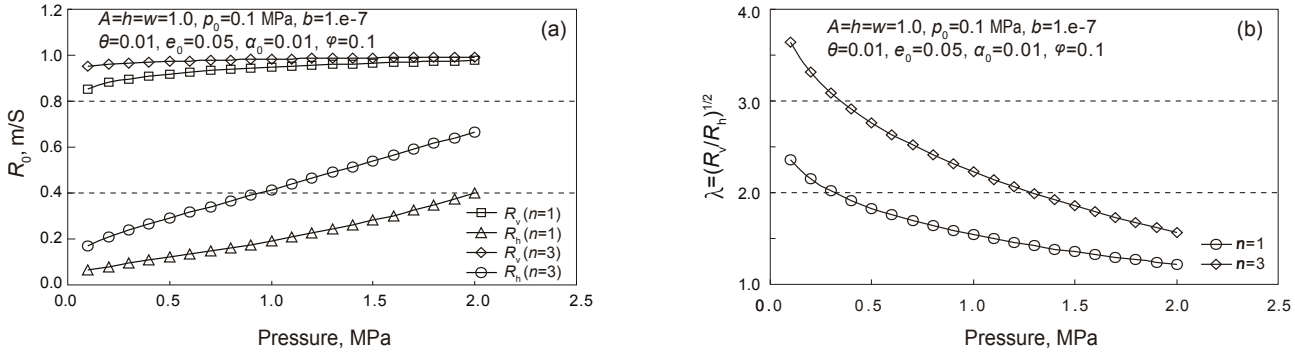

Fig. 5 Variations of resistivity and corresponding electrical anisotropy of a formation with fractures of partly closed fracture surfaces with pressure. (a) horizontal and vertical resistivities, (b) electrical anisotropy

5 Electrical responses of two sets of orthorhombic fractures in the *z*-direction

Considering the porous matrix with two sets of orthorhombic fractures in the *z*-direction, the height of the formation is h, the length is $L = L_2 + L_3$, the width is $w = w_2 + w_3$, and the fracture aperture is e. The resistivities in the three directions of x, y, z can be analyzed through the serial and parallel resistances of the elements (Ritzi et al, 1992) in Fig. 6(a). For the vertical electrical current in the *z*-direction, the resistances of the porous matrix and fractures of elements (1), (2), (3), and (4) in Fig. 6(a) are R_1, R_2, R_3 and R_4, their corresponding resistivities are ρ_1, ρ_2, ρ_3 and ρ_4, and they have relationships of

$$\begin{aligned} R_1 &= (\rho_1 h)/(w_2 L_2) \quad R_2 = (\rho_2 h)/(w_2 L_3) \\ R_3 &= (\rho_3 h)/(w_3 L_2) \quad R_4 = (\rho_4 h)/(w_3 L_3) \end{aligned} \tag{8}$$

where element (1) is the porous matrix, (2) and (3) are fracture media, (4) may be fracture fluid which means the fractures are connected with formation water, or be porous matrix which is corresponding to non-connected fractures.

The resistivity R of the fractured formation is the parallel result of the four elements, also from Ohm's law, we have:

$$\begin{aligned} R &= (1/R_1 + 1/R_2 + 1/R_3 + 1/R_4)^{-1} \\ &= R_v \cdot h / [(w_2 + w_3)(L_2 + L_3)] \end{aligned} \tag{9}$$

The vertical resistivity of the fractured formation can be derived from Eq. (9)

$$\begin{aligned} R_v = &[(w_2 + w_3)(L_2 + L_3)] \times \\ &(1/R_1 + 1/R_2 + 1/R_3 + 1/R_4)^{-1} / h \end{aligned} \tag{10}$$

For fractures connected with formation water, we have $\rho_4 = \rho_3 = \rho_1 = R_w$, from Eqs. (8) and (9), we have:

$$R_v = \frac{R_w \rho_{rb} (w_2 + w_3)(L_2 + L_3)}{w_2 L_2 R_w + (w_3 L_2 + w_2 L_3 + w_3 L_3)\rho_{rb}} \tag{11}$$

For fractures that are not connected with formation water, that is $\rho_4 = R_{rb}$, $\rho_3 = \rho_1 = R_w$, from Eqs. (8) and (9), we can obtain:

$$R_v = \frac{R_w \rho_{rb} (w_2 + w_3)(L_2 + L_3)}{(w_2 L_2 + w_3 L_3)R_w + (w_3 L_2 + w_2 L_3)\rho_{rb}} \tag{12}$$

Similar to the above vertical resistivity analysis, for the exerted electrical current in the horizontal x-direction, the resistivities of matrix and fractures of elements (1), (2), (3), and (4) in Fig. 6(a) are R_1, R_2, R_3 and R_4, and we have:

$$\begin{aligned} R_1 &= (w_2 \rho_2)/(L_2 h), R_2 = (w_2 \rho_1)/(L_3 h) \\ R_3 &= (w_3 \rho_3)/(L_2 h), R_4 = (w_3 \rho_4)/(L_3 h) \end{aligned} \tag{13}$$

The serial result of (1) and (3) is R_{13}. and that of (2) and (4) is R_{24}. From the parallel result of R_{13} and R_{24}, we have the resistance and resistivity in the x direction:

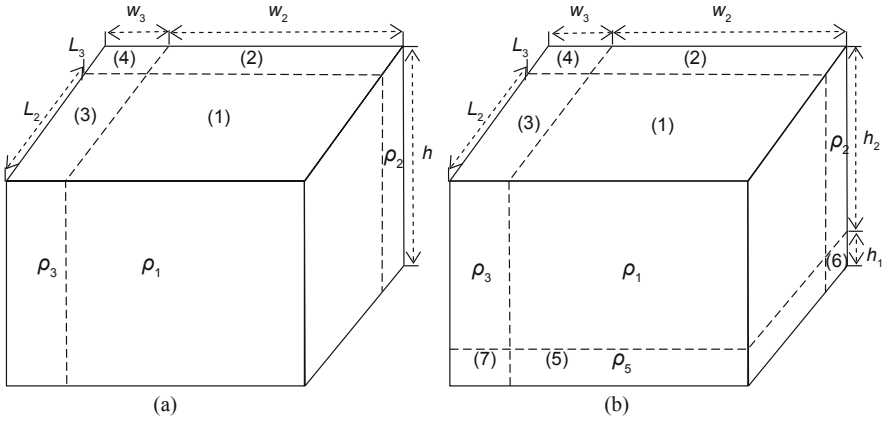

Fig. 6 Fractured formation model of multiple sets of fractures. (a) two sets of vertical fractures, (b) three sets of orthorhombic fractures

$$R=\left(1/R_{13}+1/R_{24}\right)^{-1}=\left[R_{\mathrm{hx}}\cdot(w_2+w_3)\right]/\left[h(L_2+L_3)\right] \quad (14)$$

$$R_{\mathrm{hx}}=\frac{L_2+L_3}{w_2+w_3}\left[\frac{(w_2\rho_1+w_3\rho_4)(w_2\rho_2+w_3\rho_3)}{L_2(w_2\rho_1+w_3\rho_4)+L_3(w_2\rho_2+w_3\rho_3)}\right] \quad (15)$$

For fractures connected or non-connected with formation water, from Eqs. (13) and (19), the resistivity in the *x*-direction is:

$$R_{\mathrm{hx}}=\frac{(L_2+L_3)R_{\mathrm{w}}(w_2R_{\mathrm{rb}}+w_3R_{\mathrm{w}})}{L_2(w_2+w_3)R_{\mathrm{w}}+L_3(w_2R_{\mathrm{rb}}+w_3R_{\mathrm{w}})}$$

(for connected one) (16)

$$R_{\mathrm{hx}}=\frac{L_2+L_3}{w_2+w_3}\left[\frac{(w_2R_{\mathrm{w}}+w_3R_{\mathrm{rb}})(w_2R_{\mathrm{rb}}+w_3R_{\mathrm{w}})}{L_2(w_2R_{\mathrm{w}}+w_3R_{\mathrm{rb}})+L_3(w_2R_{\mathrm{rb}}+w_3R_{\mathrm{w}})}\right]$$

(for non-connected one)

For a similar reason, for the electrical current in the horizontal y-direction, the resistivities of porous matrix and fractures of elements (1), (2), (3), and (4) are R_1, R_2, R_3 and R_4, which can be expressed as follows:

$$R_1=\left(\rho_1L_2\right)/\left(w_2h\right),\quad R_2=\left(\rho_2L_3\right)/\left(w_2h\right)$$
$$R_3=\left(\rho_3L_2\right)/\left(w_3h\right),\quad R_4=\left(\rho_4L_3\right)/\left(w_3h\right) \quad (17)$$

The parallel result of (1) and (2) is R_{12}, and that of (3) and (4) is R_{34}, resistance and resistivity in the *y* direction can be derived from the serial result of R_{12} and R_{34}:

$$R=\left(1/R_{12}+1/R_{34}\right)^{-1}=\left[R_{\mathrm{hy}}(L_2+L_3)\right]/\left[h(w_2+w_3)\right] \quad (18)$$

$$R_{\mathrm{hy}}=\frac{w_2+w_3}{L_2+L_3}\left[\frac{(L_2\rho_1+L_3\rho_2)(L_2\rho_3+L_3\rho_4)}{w_2(L_2\rho_3+L_3\rho_4)+w_3(L_2\rho_1+L_3\rho_2)}\right] \quad (19)$$

For fractures connected or non-connected with formation water, we have resistivity in the *y*-direction as follows:

$$R_{\mathrm{hy}}=\frac{(w_2+w_3)R_{\mathrm{w}}(L_2R_{\mathrm{rb}}+L_3R_{\mathrm{w}})}{w_2R_{\mathrm{w}}(L_2+L_3)+w_3(L_2R_{\mathrm{rb}}+L_3R_{\mathrm{w}})}$$

(for connected one) (20)

$$R_{\mathrm{hy}}=\frac{w_2+w_3}{L_2+L_3}\left[\frac{(L_2R_{\mathrm{rb}}+L_3R_{\mathrm{w}})(L_2R_{\mathrm{w}}+L_3R_{\mathrm{rb}})}{w_2(L_2R_{\mathrm{w}}+L_3R_{\mathrm{rb}})+w_3(L_2R_{\mathrm{rb}}+L_3R_{\mathrm{w}})}\right]$$

(for non-connected one)

Fig. 7 and Fig. 8 show the comparison of resistivities and electrical anisotropy changing with the conductivity of formation water in a formation with a single set of vertical fractures of fixed aperture and in two sets of orthorhombic fractures of variable aperture for a specific matrix porosity.

Fig. 7 indicates that in a vertical fractured formation, there are differences in electrical anisotropy in different directions, so the azimuthal resistivity measurements can be applied to determining the fracture strikes. Fig. 8 shows the results of two sets of vertical fractures of variable apertures for a specific matrix porosity, and the fracture distributed along the *x*-axis has a larger aperture than the fracture distributed along the *y*-axis. From Fig. 8(a) it is seen that the resistivity of the *y* direction is higher than that of the *x* direction, and the electrical anisotropy of horizontal directions *x*, *y* are less than 1.0 in Fig. 8(b). Therefore, if a suitable survey configuration is used, the vertical fractures can be detected theoretically.

6 Electrical anisotropic responses of formation with three sets of orthorhombic fractures

Considering the model with three sets of orthorhombic fractures in Fig. 6(b), if the exerted electrical current is in the *z* direction, the horizontal and vertical resistivities can be analyzed through separating the model into two parts as shown in Fig. 9(a) and (b), the resistivity can be calculated through two serial parts. The upper one is composed of four elements of (1), (2), (3) and (4), and they are parallel

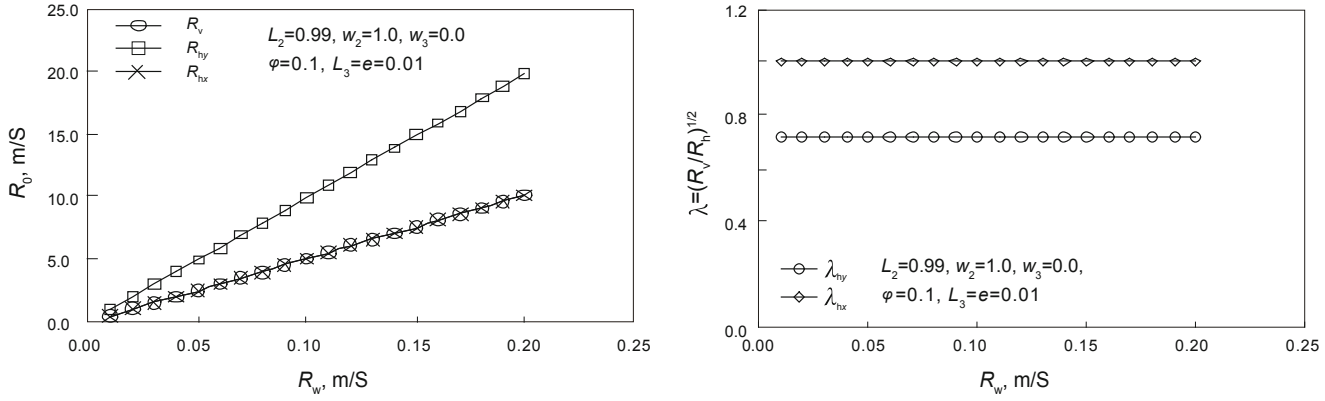

Fig. 7 Variation of the electrical anisotropy with the conductivity of formation water in a formation with a single set of vertical fractures of fixed aperture for a specific matrix porosity. (a) resistivities of three directions *x*, *y*, *z*, (b) electrical anisotropy of horizontal directions *x*, *y*

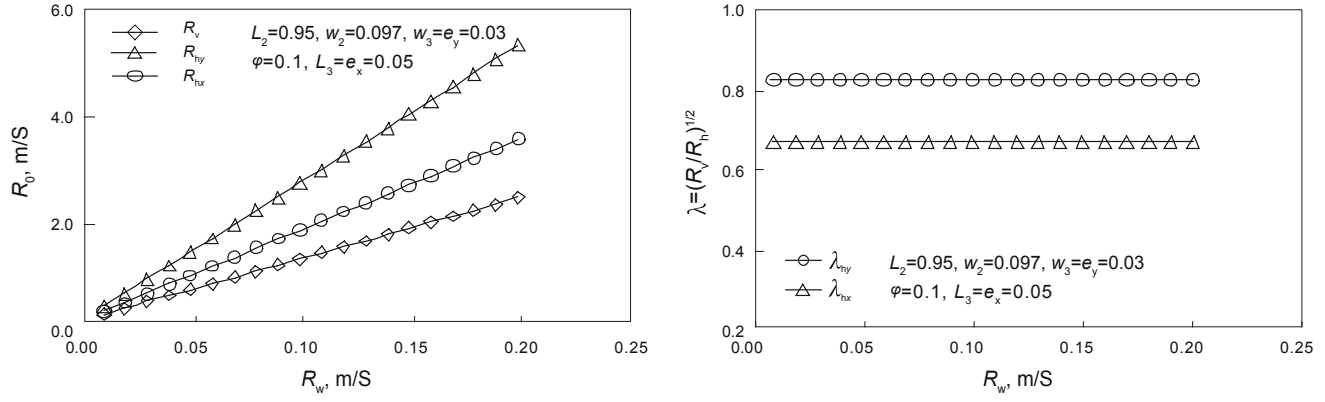

Fig. 8 Variation of the electrical anisotropy with conductivity of formation water in a formation with two sets of orthorhombic fractures of variable aperture for a specific matrix porosity. (a) resistivities of three directions *x*, *y*, *z*, (b) electrical anisotropy of horizontal directions *x*, *y*

conductive; the lower one is composed of four elements of (5), (6), (7), and (8), and they are also parallel conductive (Campbell, 1977).

$$R_1=(\rho_1 h_2)/(L_2 w_2),\ R_2=(\rho_2 h_2)/(L_3 w_2)$$
$$R_3=(\rho_3 h_2)/(L_2 w_3),\ R_4=(\rho_4 h_2)/(L_3 w_3) \tag{21}$$

$$R_5=(\rho_5 h_1)/(L_2 w_2),\ R_6=(\rho_6 h_1)/(L_3 w_2)$$
$$R_7=(\rho_7 h_1)/(L_2 w_3),\ R_8=(\rho_8 h_1)/(L_3 w_3) \tag{22}$$

where R_i, (i=1, 2,⋯, 8) represents the resistance of the eight elements in Fig. 9, in unit of S, ρ_i, (i=1, 2,⋯, 8) represents corresponding resistivity in inverse of S/m.

The resistances of the upper part R_u and the lower part R_d can be rewritten as:

$$R_u=\left[1/R_1+1/R_2+1/R_3+1/R_4\right]^{-1}$$
$$R_d=\left[1/R_5+1/R_6+1/R_7+1/R_8\right]^{-1} \tag{23}$$

The resistance of the fractured formation R is the serial result of R_u and R_d, and we have:

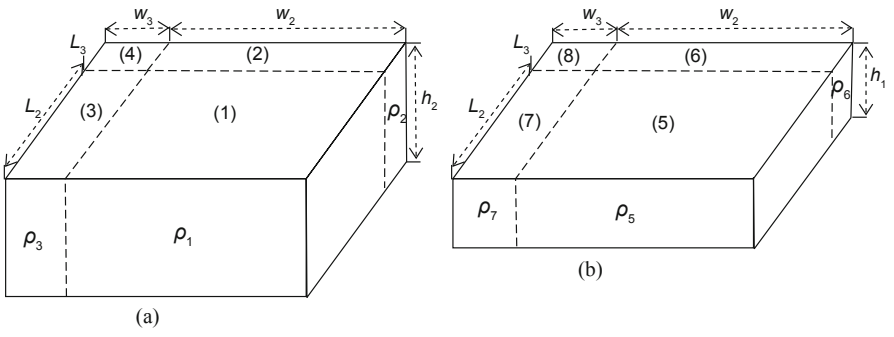

Fig. 9 Upper and lower parts of the three sets of orthorhombic fracture model. (a) parameters of the elements of the upper part, (b) parameters of the elements of the lower part

$$R = R_u + R_d = \left[R_v \left(h_1 + h_2 \right) \right] / \left[(L_2 + L_3)(w_2 + w_3) \right] \quad (24)$$

Correspondingly, the vertical resistivity R_v is

$$R_v = \frac{(L_2 + L_3)(w_2 + w_3)}{\left(h_1 + h_2 \right)} \times \left[\frac{h_2 \rho_1 \rho_2 \rho_3 \rho_4}{L_2 w_2 \rho_2 \rho_3 \rho_4 + L_3 w_2 \rho_1 \rho_3 \rho_4 + L_2 w_3 \rho_1 \rho_2 \rho_4 + L_3 w_3 \rho_1 \rho_2 \rho_3} + \frac{h_1 \rho_5 \rho_6 \rho_7 \rho_8}{L_2 w_2 \rho_6 \rho_7 \rho_8 + L_3 w_2 \rho_5 \rho_7 \rho_8 + L_2 w_3 \rho_5 \rho_6 \rho_8 + L_3 w_3 \rho_5 \rho_6 \rho_7} \right] \quad (25)$$

If the fractures of different sets are connected or non-connected with the formation water, the above vertical resistivity R_v can be simplified to:

$$R_v = \frac{(L_2 + L_3)(w_2 + w_3)}{\left(h_1 + h_2 \right)} \times \left[\frac{h_2 R_{rb} R_w}{L_2 w_2 R_w + L_3 w_2 R_{rb} + L_2 w_3 R_{rb} + L_3 w_3 R_{rb}} + \frac{h_1 R_w}{L_2 w_2 + L_3 w_2 + L_2 w_3 + L_3 w_3} \right] \quad (26)$$

(for connected one)

$$R_v = \frac{(L_2 + L_3)(w_2 + w_3)}{\left(h_1 + h_2 \right)} \times \left[\frac{h_2 R_{rb} R_w}{L_2 w_2 R_w + L_3 w_2 R_{rb} + L_2 w_3 R_{rb} + L_3 w_3 R_{rb}} + \frac{h_1 R_{rb}}{L_2 w_2 + L_3 w_2 + L_2 w_3 + L_3 w_3} \right] \quad (27)$$

(for non-connected one)

For the exerted electrical current in the horizontal *x*-direction, the resistivity can be analyzed through two parts. The left one is composed of four elements of (3), (4), (7), and (8), and they are parallel conductive; the right one is composed of four elements of (1), (2), (5), and (6), and they are also parallel conductive. Using the serial result of the left and right parts (Appendix B), we can obtain horizontal resistivities in the *x*-direction with connected or non-connected fractures.

$$R_{hx} = \frac{\left[(h_1 + h_2)(L_2 + L_3) \right]}{\left(w_2 + w_3 \right)} \times \left[\frac{w_3 R_w}{\left(L_2 + L_3 \right)(w_2 + w_3)} + \frac{w_2 R_w R_{rb}}{L_2 h_2 R_w + (L_3 h_2 + L_2 h_1 + L_3 h_1) R_w} \right] \quad (28)$$

(for connected one)

$$R_{hx} = \frac{\left[(h_1 + h_2)(L_2 + L_3) \right]}{\left(w_2 + w_3 \right)} \times \left[\frac{w_3 R_{rb} R_w}{L_2 h_2 R_{rb} + (L_3 h_2 + L_2 h_1 + L_3 h_1) R_w} + \frac{w_2 R_{rb} R_w}{(L_2 h_2 + L_3 h_1) R_w + (L_3 h_2 + L_2 h_1) R_{rb}} \right] \quad (29)$$

(for non-connected one)

When the exerted electrical current is in the horizontal *y*-direction, the resistivity can be analyzed through two parts. The front one is composed of four elements of (1), (3), (5), and (7), and they are parallel conductive; the back one is composed of four elements of (2), (4), (6), and (8), and they are also parallel conductive. Using the serial result of the front and back parts (Appendix C), we have horizontal resistivities in the *y*-direction with connected or non-connected fractures.

$$R_{hy} = \frac{\left[(h_1 + h_2)(w_2 + w_3) \right]}{\left(L_2 + L_3 \right)} \times \left[\frac{L_2 R_{rb} R_w}{w_2 h_2 R_w + \left(w_3 h_2 + w_2 h_1 + w_3 h_1 \right) R_{rb}} + \frac{L_3 R_w}{(h_1 + h_2)(w_2 + w_3)} \right] \quad (30)$$

(for connected one)

$$R_{hy} = \frac{\left[(h_1 + h_2)(w_2 + w_3) \right]}{\left(L_2 + L_3 \right)} \times \left[\frac{L_2 R_{rb} R_w}{\left(w_2 h_2 + w_3 h_1 \right) R_w + (w_3 h_2 + w_2 h_1) R_{rb}} + \frac{L_3 R_{rb} R_w}{w_2 h_2 R_{rb} + (w_3 h_2 + w_2 h_1 + w_3 h_1) R_w} \right] \quad (31)$$

(for non-connected one)

Fig. 10(a) and Fig. 10(b) show resistivity and electrical anisotropy changing with resistivity of the formation water in a formation with three sets of orthorhombic fractures of different fracture apertures at a specific matrix porosity. The fractures distributed along the *x*-axis and those along the *z*-axis have the same aperture that are larger than the aperture of the fractures along the *y*-axis. From Fig. 10(a) it is seen that the resistivity of the *y* direction is higher than that of the *x* direction, whereas the resistivity in the *z*-direction has the lowest value as there are two sets of fractures which extend in this direction. Because of the fractures in the vertical *z*-direction, the electrical anisotropy of horizontal directions *x*, *y* are less than 1.0. Therefore, even in complex fracture distributions, if a suitable survey configuration is used, fractures in different strikes can be surveyed by using electrical exploration.

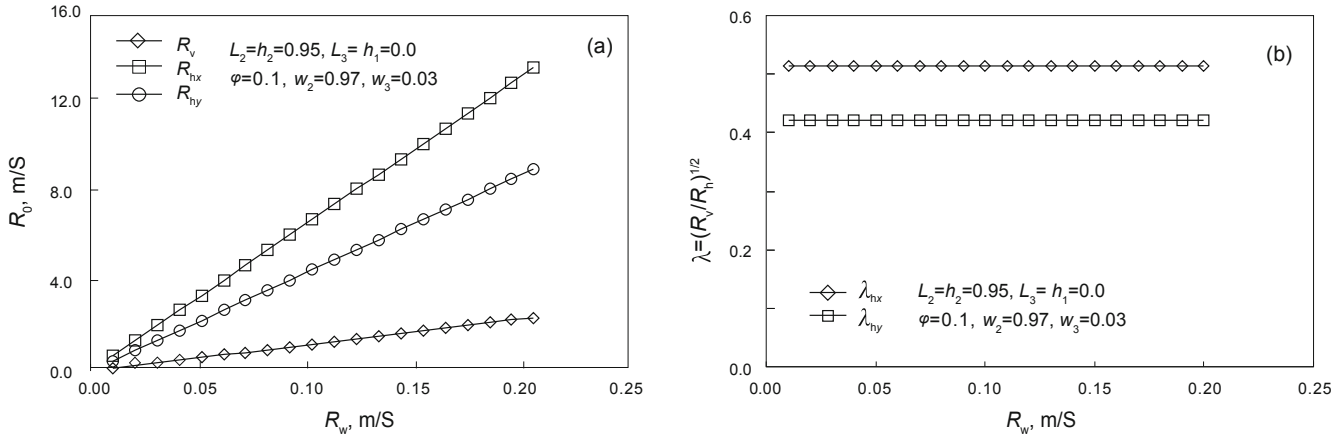

Fig. 10 Variation of resistivity and electrical anisotropy with the resistivity of formation water in a formation with three sets of orthorhombic fractures of variable apertures at a specific matrix porosity. (a) resistivity of three directions x, y, z, (b) electrical anisotropy of horizontal directions x, y

7 Electrical anisotropic responses of porous formation with multiple sets of slanting fractures

For the integrity of the discussion, here we consider a formation with three sets of slanting fractures, and fracture surfaces intersect the z axis with angles of α_1, α_2 and α_3, the strikes of three fracture surfaces intersect the x axis with angles of β_1, β_2 and β_3. The fractured formation indicates azimuthal anisotropy, that is to say, the non-diagonal elements in the resistivity tensor are not zero. The resistivity tensor can be derived from the horizontal and vertical resistivities of the horizontal fracture model or orthorhombic fracture model by the following rotational transformation (Senos Matias, 2002):

$$\hat{\sigma}_{\mathrm{fr}}^{(0)}=\begin{bmatrix}\sigma_x & 0 & 0\\ 0 & \sigma_y & 0\\ 0 & 0 & \sigma_z\end{bmatrix}=\begin{bmatrix}\rho_{\mathrm{hx}}^{-1} & 0 & 0\\ 0 & \rho_{\mathrm{hy}}^{-1} & 0\\ 0 & 0 & \rho_{\mathrm{v}}^{-1}\end{bmatrix} \tag{32}$$

where $\hat{\sigma}_{\mathrm{fr}}^{(0)}$is the conductivity tensor of the horizontal fracture model or orthorhombic fracture model, σ_x, σ_y, and σ_z are conductivities in the x, y and z directions, ρ_{hx}, ρ_{hy}, and ρ_{hz} are resistivities in the corresponding directions.

The conductivity tensor of the fractured formation with multiple sets of slanting fractures is (Senos Matias, 2002):

$$\sigma_{\mathrm{fr}}^{(\alpha_i)}=T_{\alpha_i}^{-1}\sigma_{\mathrm{fr}}^{(\alpha_{i-1})}T_{\alpha_i} \tag{33}$$

where $\sigma_{\mathrm{fr}}^{(\alpha_0)}=\sigma_{\mathrm{fr}}^{(0)}$

$$T_{\alpha_i}=\begin{bmatrix}\cos\alpha_i\cos\beta_i & \cos\alpha_i\sin\beta_i & -\sin\alpha_i\\ -\sin\beta_i & \cos\beta_i & 0\\ \sin\alpha_i\cos\beta_i & \sin\alpha_i\sin\beta_i & \cos\alpha_i\end{bmatrix}(i=1,2,3)$$

8 Conclusions

1) For a specific fracture porosity, the higher the matrix porosity, the weaker the electrical anisotropy. Therefore, if the portion of the fracture porosity in the fractured formation is very low, the electrical anisotropy caused by the existence of fractures can be ignored and the formation can be treated as an isotropic one.

2) For a specific matrix porosity, the wider the fracture aperture or the larger the fracture density, the stronger the electrical anisotropy. Furthermore, the stronger the closed fracture roughness or the larger the closed contact area, the weaker the electrical anisotropy in the fractured formation.

3) For a fractured formation with closed, rough surfaces, the electrical anisotropy increases non-linearly with the increase of the fracture porosity. For a specific total porosity in the formation, the higher the proportion of the fracture porosity, the stronger the electrical anisotropy. In commonly encountered fractured formations, electrical anisotropy may be as high as 15 or more.

4) For a fractured formation of partly closed rough surfaces, the horizontal and vertical resistivities increase non-linearly with the elasticity and fracture density of the formation and the confining pressure on the formation, whereas electrical anisotropy shows the opposite variation.

5) For the multiple sets of orthorhombic fractures, because of the variation of fracture aperture, fracture density and partly closed contact area in each set, variations of the resistivities and electrical anisotropy are complex, but the above characteristics still hold.

Acknowledgements

We appreciate the constructive help and encouragement of Dr. Xiangyang Li in the British Geological Survey. The authors also would like to acknowledge the support of the National Basic Research Program (973 Program) (2007CB209607) of China, National High-tech R&D Program (863 Program) (2007AA060502) and the Fundamental Research Project (07A10303) of CNPC.

References

Al Hagrey S A. Electric study of fracture anisotropy at Falkenberg, Germany. Geophysics. 1994. 59(6): 881-888

Archie G E. The Electrical resistivity log as an aid in determining some reservoir characteristics. Trans. AIME. 1942. 146: 54-62

Berg C R. A simple, effective-medium model for water saturation in porous rocks. Geophysics. 1995. 60(4): 1070-1080

Boadu F K, Gyamfi J and Owusu E. Determining subsurface fracture characteristics from azimuthal resistivity surveys: A case study at Nsawam, Ghana. Geophysics. 2005. 70(5): B35-B42

Brace W F and Orange A S. Electrical resistivity changes in saturated rocks during fracture and frictional sliding. Journal of Geophysical Research. 1968. 73: 1433-1445

Brown S R. Simple mathematical model of a rough fracture. Journal of Geophysical Research. 1995. 100(B4): 5941-5952

Busby J P. The effectiveness of azimuthal apparent-resistivity measurements as a method for determining fracture strike orientations. Geophysical Prospecting. 2000. 48(4): 677-695

Bussian A E. Electric conductance in a porous medium. Geophysics. 1983. 48(9): 1258-1268

Campbell D L. Model for estimating electric macroanisotropy coefficient of aquifers with horizontal and vertical fractures (short note). Geophysics. 1977. 42(1): 114-117

Carpenter P J, Keeley M C and Kaufmann R S. Azimuthal resistivity surveys over a fractured landfill cover. Bulletin of the Association of Engineering Geologists. 1994. 31(1): 123-131

Chapman M. Frequency-dependent anisotropy due to meso-scale fractures in the presence of equant porosity. Geophysical Prospecting. 2003. 51(5): 369-379

Cohn M E and Rudman A J. Orientation of near-surface fractures from azimuthal measurements of apparent resistivity. SEG Expanded Abstracts. 1995. 14(NS1): 372-374

Colin M S. Seismic characterization of reservoirs containing multiple fracture sets. SEG Expanded Abstracts. 2007. 26: 329-333

Horne S. Fracture characterization from walkaround VSPs. Geophysical Prospecting. 2003. 51(6): 493-499

Lane J W, Haeni F P and Watson W M. Use of a square-array direct-current resistivity method to detect fractures in crystalline bedrock in New Hampshire. Ground Water. 1995. 33(3): 476-485

Linde N, Binley A, Ari T, et al. Improved hydrogeophysical characterization using joint inversion of cross-hole electrical resistance and ground-penetrating radar traveltime data. Water Resources Research. 2006. 42(12): 2404-2409

Lucia F J. Carbonate Reservoir Characterization: An Integrated Approach. Publisher: Springer. 2007. 1-36

Luthi S M and Souhaite P. Fracture apertures from electrical borehole scans. Geophysics. 1990. 55(7): 821-833

Meju M A, Fontes S L, Ulugergerli E U, et al. A joint TEM-HLEM geophysical approach to borehole siting in deeply weathered granitic terrains. Ground Water. 2001. 39(4): 554-567

Meju M A. Geoelectromagnetic exploration for natural resources: models, case studies and challenges. Surveys in Geophysics. 2002. 23(2-3): 133-205

Minh C C, Clavaud J B, Sundararaman P, et al. Graphical analysis of laminated sand-shale formations in the presence of anisotropic shales. SPWLA 48th Annual Logging Symposium. 2007. paper MM

Ritzi R W and Andolsek R H. Relation between anisotropic transmissivity and azimuthal resistivity surveys in shallow, fractured, carbonate flow systems. Ground Water. 1992. 30(5): 774-780

Senos Matias M J. Square array anisotropy measurements and resistivity sounding interpretation. Journal of Applied Geophysics. 2002. 49(3): 185-194

Shaw R K and Sen M K. Born integral, stationary phase and linearized reflection coefficients in weak anisotropic media. Geophysical Journal International. 2004. 158(1): 225-238

Shaw R K and Sen M K. Use of AVOA data to estimate fluid indicator in a vertically fractured medium. Geophysics. 2006. 71(3): C15-C24

Standen E, Nurmi R, El-Wazeer F, et al. Quantitative applications of wellbore images to reservoir analysis. Transactions of the 34th SPWLA. 1993. Paper EEE

Stesky R M. Electrical conductivity of brine-saturated fractured rock. Geophysics. 1986. 51(8): 1585-1593

Tetsuya T, Kazuhiko T and Takatoshi N. Fracture network modeling using electrical borehole images. Transactions of the 43rd SPWLA. 2002. Paper FF

Thomsen L. Weak elastic anisotropy. Geophysics. 1986. 51(10): 1954-1966

Tryggvason A and Linde N. Local earthquake (LE) tomography with joint inversion for P- and S-wave velocities using structural constraints. Geophysical Research Letters. 2006. 33(7): 303-315

Walsh J B. Effect of pore pressure and confining pressure on fracture permeability. Int. J. Rock Mech. Min. Sci. Geomech. Abstr. 1981. 18: 429-435

Waxman M H and Smits L J M. Electrical conductivities in oil-bearing shaly sands. The Society of Petroleum Engineers' Journal. 1968. 8: 107-122

Appendix A: Resistivity equation of a fractured porous formation with multiple sets of horizontal fractures

Referring to Fig. 2, when the exerted electrical current is in the horizontal direction, the porous matrix and fractures have resistivities of $R_{\mathrm{r}}^{\mathrm{h}}$ and $R_{\mathrm{f}i}^{\mathrm{h}}$ respectively:

$$R_{\mathrm{r}}^{\mathrm{h}} = \rho_{\mathrm{r}} w \Big/ \left[(h - \sum_{i=1}^{n} e_i) L \right], \quad R_{\mathrm{f}i}^{\mathrm{h}} = R_{\mathrm{w}} w / (e_i L) \tag{A-1}$$

The horizontal resistance $R_{\mathrm{rf}}^{\mathrm{h}}$ and resistivity R_{h} of the fractured porous formation can be expressed as:

$$\begin{aligned} R_{\mathrm{rf}}^{\mathrm{h}} &= \rho_{\mathrm{rf}}^{\mathrm{h}} w/(hL) = \left[1/R_{\mathrm{r}}^{\mathrm{h}} + \sum_{i=1}^{n} \left(1/R_{\mathrm{f}i}^{\mathrm{h}} \right) \right]^{-1} \\ R_{\mathrm{h}} &= \frac{\rho_{\mathrm{r}} R_{\mathrm{w}}}{(\rho_{\mathrm{r}} - R_{\mathrm{w}}) new / A + R_{\mathrm{w}}} \end{aligned} \tag{A-2}$$

For the same reason, when the exerted electrical current is in the vertical direction, the porous matrix and fractures have resistivities of $R_{\mathrm{r}}^{\mathrm{v}}$ and $R_{\mathrm{f}i}^{\mathrm{v}}$ respectively:

$$\begin{aligned} R_{\mathrm{r}}^{\mathrm{v}} &= \rho_{\mathrm{r}} (h - \sum_{i=1}^{n} e_i) / (wL) \\ R_{\mathrm{f}i}^{\mathrm{v}} &= R_{\mathrm{w}} e_i / (wL) \end{aligned} \tag{A-3}$$

The vertical resistance $R_{\mathrm{rf}}^{\mathrm{v}}$ and resistivity R_{v} of the fractured porous formation can be expressed as:

$$\begin{aligned} R_{\mathrm{rf}}^{\mathrm{v}} &= \rho_{\mathrm{rf}}^{\mathrm{v}} h / (wL) = R_{\mathrm{r}}^{\mathrm{v}} + \sum_{i=1}^{n} R_{\mathrm{f}i}^{\mathrm{v}} \ \ (wh = A) \\ R_{\mathrm{v}} &= \rho_{\mathrm{r}} + \frac{new(R_{\mathrm{w}} - \rho_{\mathrm{r}})}{A} \end{aligned} \tag{A-4}$$

where n is the total fracture number, e is the fracture aperture, w is the extended width of the fracture, L is the extended

length of the fracture, h is the thickness of the formation, $wh=A$ is the area of the formation section, and n=1means the formation has a single fracture.

Appendix B: Horizontal resistivity in the *x*-direction of fractured formation with three sets of orthorhombic fractures

Referring to Fig. 8, when the exerted electrical current is in the horizontal x-direction, the resistivity can be analyzed through two parts, left and right. The left part is composed of four elements of (3), (4), (7), and (8), and they are parallel conductive; the right one is composed of four elements of (1), (2), (5), and (6), and they are also parallel conductive.

$$\begin{aligned} R_1 &= (\rho_1 w_2)/(h_2 L_2),\ R_2 = (\rho_2 w_2)/(h_2 L_3) \\ R_3 &= (\rho_3 w_3)/(L_2 h_2),\ R_4 = (\rho_4 w_3)/(L_3 h_2) \end{aligned} \tag{B-1}$$

$$\begin{aligned} R_5 &= (\rho_5 w_2)/(h_1 L_2),\ R_6 = (\rho_6 w_2)/(h_1 L_3) \\ R_7 &= (\rho_7 w_3)/(L_2 h_1),\ R_8 = (\rho_8 w_3)/(L_3 h_1) \end{aligned} \tag{B-2}$$

The resistances of the left part R_l and that of the right part R_r can be rewritten as:

$$\begin{aligned} R_l &= \left[1/R_3 + 1/R_4 + 1/R_7 + 1/R_8\right]^{-1} \\ R_r &= \left[1/R_1 + 1/R_2 + 1/R_5 + 1/R_6\right]^{-1} \end{aligned} \tag{B-3}$$

The resistance of the fractured porous formation is the serial result of the two parts, and from Ohm's law, we can obtain:

$$R = R_l + R_r = \left[R_{hx}(w_2 + w_3)\right]/\left[(h_1 + h_2)(L_2 + L_3)\right] \tag{B-4}$$

From Eq. (B-4), the horizontal resistivity R_{hx} in the x-direction of the fractured porous formation is:

$$\begin{aligned} R_{hx} = {} & \frac{\left[(h_1 + h_2)(L_2 + L_3)\right]}{(w_2 + w_3)} \times \\ & \left[\frac{w_3}{L_2 h_2/\rho_3 + L_3 h_2/\rho_4 + L_2 h_1/\rho_7 + L_3 h_1/\rho_8} \right. \\ & \left. + \frac{w_2}{L_2 h_2/\rho_1 + L_3 h_2/\rho_2 + L_2 h_1/\rho_5 + L_3 h_1/\rho_6}\right] \end{aligned} \tag{B-5}$$

If the fractures of different sets are connected with formation water, that is $\rho_4 = \rho_3 = \rho_2 = R_w$, $\rho_5 = \rho_6 = \rho_7 = \rho_8 = R_w$, $\rho_1 = R_{rb}$ and inserting them into Eq. (B-5), we have:

$$\begin{aligned} R_{hx} = {} & \frac{\left[(h_1 + h_2)(L_2 + L_3)\right]}{(w_2 + w_3)} \left[\frac{w_3 R_w}{(L_2 + L_3)(w_2 + w_3)} \right. \\ & \left. + \frac{w_2 R_w R_{rb}}{L_2 h_2 R_w + (L_3 h_2 + L_2 h_1 + L_3 h_1) R_w}\right] \end{aligned} \tag{B-6}$$

If the fractures of different sets are non-connected with formation water, that is, $\rho_5 = \rho_3 = \rho_2 = R_w$, $\rho_4 = \rho_6 = \rho_7 = \rho_8 = R_{rb}$, $\rho_1 = R_{rb}$, and inserting them into Eq. (B-5), we have:

$$\begin{aligned} R_{hx} = {} & \frac{\left[(h_1 + h_2)(L_2 + L_3)\right]}{(w_2 + w_3)} \left[\frac{w_3 R_{rb} R_w}{L_2 h_2 R_{rb} + (L_3 h_2 + L_2 h_1 + L_3 h_1) R_w} \right. \\ & \left. + \frac{w_2 R_{rb} R_w}{(L_2 h_2 + L_3 h_1) R_w + (L_3 h_2 + L_2 h_1) R_{rb}}\right] \end{aligned} \tag{B-7}$$

Appendix C: Horizontal resistivity in the *y*-direction of fractured formation with three sets of orthorhombic fractures

When the exerted electrical current is in the horizontal y-direction, the resistivity can be analyzed through two parts, front and back. The front part is composed of four elements of (1), (3), (5), and (7), and they are parallel conductive; the back one is composed of four elements of (2), (4), (6), and (8), and they are also parallel conductive.

$$\begin{aligned} R_1 &= (\rho_1 L_2)/(h_2 w_2),\ R_2 = (\rho_2 L_3)/(h_2 w_2) \\ R_3 &= (\rho_3 L_2)/(w_3 h_2),\ R_4 = (\rho_4 L_3)/(w_3 h_2) \end{aligned} \tag{C-1}$$

$$\begin{aligned} R_5 &= (\rho_5 L_2)/(h_1 w_2),\ R_6 = (\rho_6 L_3)/(h_1 w_2) \\ R_7 &= (\rho_7 L_2)/(w_3 h_1),\ R_8 = (\rho_8 L_3)/(w_3 h_1) \end{aligned} \tag{C-2}$$

The resistances of the front part R_f and that of the back part R_b can be rewritten as:

$$\begin{aligned} R_f &= \left[1/R_1 + 1/R_3 + 1/R_5 + 1/R_7\right]^{-1} \\ R_b &= \left[1/R_2 + 1/R_4 + 1/R_6 + 1/R_8\right]^{-1} \end{aligned} \tag{C-3}$$

The resistances of the fractured porous formation is the serial result of the two parts, and from Ohm's law, we can obtain:

$$R = R_f + R_b = \left[R_{hy}(L_2 + L_3)\right]/\left[(w_2 + w_3)(h_1 + h_2)\right] \tag{C-4}$$

Inserting Eqs. (C-1), (C-2) and (C-3) into Eq. (C-4), we have:

$$R_{hy}=\frac{\left[(h_1+h_2)(w_2+w_3)\right]}{\left(L_2+L_3\right)}\times \left[\frac{L_2}{w_2h_2/\rho_1+w_3h_2/\rho_3+w_2h_1/\rho_5+w_3h_1/\rho_7}+\frac{L_3}{w_2h_2/\rho_2+w_3h_2/\rho_4+w_2h_1/\rho_6+w_3h_1/\rho_8}\right] \quad \text{(C-5)}$$

If the fractures of different sets are connected with formation water, that is, $\rho_4=\rho_3=\rho_2=R_w$, $\rho_5=\rho_6=\rho_7=\rho_8=R_w$, $\rho_1=R_{rb}$, and inserting them into Eq. (C-5), we have:

$$R_{hy}=\frac{\left[(h_1+h_2)(w_2+w_3)\right]}{\left(L_2+L_3\right)}\left[\frac{L_3R_w}{(h_1+h_2)(w_2+w_3)}+\frac{L_2R_{rb}R_w}{w_2h_2R_w+\left(w_3h_2+w_2h_1+w_3h_1\right)R_{rb}}\right] \quad \text{(C-6)}$$

If the fractures of different sets are not connected with formation water, that is, $\rho_5=\rho_3=\rho_2=R_w$, $\rho_4=\rho_6=\rho_7=\rho_8=R_{rb}$, $\rho_1=R_{rb}$, and inserting them into Eq. (C-5), we have:

$$R_{hy}=\frac{\left[(h_1+h_2)(w_2+w_3)\right]}{\left(L_2+L_3\right)}\times \left[\frac{L_2R_{rb}R_w}{\left(w_2h_2+w_3h_1\right)R_w+(w_3h_2+w_2h_1)R_{rb}}+\frac{L_3R_{rb}R_w}{w_2h_2R_{rb}+(w_3h_2+w_2h_1+w_3h_1)R_w}\right] \quad \text{(C-7)}$$

(Edited by Hao Jie)